Journal of Molecular Structure 1036 (2013) 318–325

Contents lists available at SciVerse ScienceDirect

Journal of Molecular Structure

journal homepage: www.elsevier.com/locate/molstruc

Characterization and structural analysis of the potent antiparasitic and antiviral agent tizoxanide

Flavia P. Bruno [a], Mino R. Caira [b], Eliseo Ceballos Martin [a], Gustavo A. Monti [c], Norma R. Sperandeo [a,*]

[a] Departamento de Farmacia, Facultad de Ciencias Químicas, Universidad Nacional de Córdoba, Haya de la Torre y Medina Allende, Ciudad Universitaria, X5000HUA Córdoba, Argentina
[b] Department of Chemistry, University of Cape Town, Rondebosch 7701, South Africa
[c] Facultad de Astronomía, Matemática y Física, Universidad Nacional de Córdoba and IFEG-CONICET, Ciudad Universitaria, X5000HUA Córdoba, Argentina

HIGHLIGHTS

- The crystal structure of unsolvated tizoxanide (TIZ) was resolved.
- This modification of TIZ has a 'graphitic' structure.
- The various spectroscopic data were consistent with the resolved structure.
- The behavior on heating of TIZ was studied by DSC, TG and HSM.
- TIZ decomposes above 270 °C and no isolated melting event was detected.

GRAPHICAL ABSTRACT

Tizoxanide [2-(Hydroxy)-*N*-(5-nitro-thiazolyl)benzamide, TIZ],a new potent anti-infective agent, has been structurally characterized by X-ray analysis, solid-state NMR, DRIFT, FTRaman and Thermal Analysis. This modification of TIZ has relatively high thermal stability as a solid and a 'graphitic' structure, and is composed of tightly packed layers of extensively hydrogen bonded molecules.

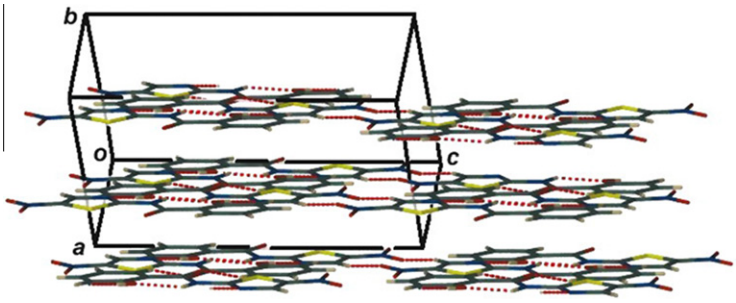

ARTICLE INFO

Article history:
Received 13 October 2012
Received in revised form 3 December 2012
Accepted 3 December 2012
Available online 10 December 2012

Keywords:
Crystal structure
^{13}C CPMAS NMR
DRIFT
FT-Raman
Thermal analysis
Tizoxanide

ABSTRACT

Tizoxanide [2-(hydroxy)-*N*-(5-nitro-2-thiazolyl)benzamide, TIZ] is a new potent anti-infective agent which may enhance current therapies for leishmaniasis, Chagas disease and viral hepatitis. The aim of this study was to identify the conformational preferences that may be related to the biological activity of TIZ by resolving its crystal structure and characterizing various physicochemical properties, including its experimental vibrational and ^{13}C nuclear magnetic resonance properties, behavior on heating and solubility in several solvents at 25 °C. TIZ crystallizes from dimethylformamide as the carboxamide tautomer in the triclinic system, space group $P(-1)$ (No. 2) with the following unit cell parameters at 173(2) K: a = 5.4110(3) Å, b = 7.3315(6) Å, c = 13.5293(9) Å, α = 97.528(3), β = 95.390(4), γ = 97.316(5), V = 524.41(6) Å^3, Z = 2, D_c = 1.680 g/cm^3, R_1 = 0.0482 and wR_2 = 0.0911 for 2374 reflections. This modification of TIZ has a 'graphitic' structure and is composed of tightly packed layers of extensively hydrogen-bonded molecules. The various spectroscopic data [Diffuse Fourier transform infrared (DRIFT) and FT-Raman, recorded in the range 3600–500 and 4000–200 cm^{-1} respectively, and solid-state ^{13}C NMR] were consistent with the structure determined by X-ray crystallography. From DSC, TG and thermomicroscopy, it was concluded that TIZ is thermally stable as a solid and that melting is not an isolated event from the one-step thermal decomposition that it undergoes above 270 °C. This modification of TIZ is practically insoluble in water and slightly soluble in polar aprotic solvents such as dimethylsulfoxide, dimethylformamide and dioxane.

* Corresponding author.
E-mail address: nrscor@fcq.unc.edu.ar (N.R. Sperandeo).

0022-2860/$ - see front matter © 2012 Elsevier B.V. All rights reserved.
http://dx.doi.org/10.1016/j.molstruc.2012.12.004

1. Introduction

Parasitic and viral diseases such as leishmaniasis, trypanosomiasis and hepatitis C represent a serious problem to the health and economy of many countries. There are an estimated annual 1.5–2.0 million new cases of leishmaniasis, of which approximately 500,000 belong to the potentially fatal visceral form [1]. The American trypanosomiasis (Chagas disease) affects approximately 15–20 million people from Southern California to Argentina and Chile; 2–3% of the Latin American (LA) population is infected, encompassing a burden of about 670,000 Disability Adjusted Life Years (DALYs), and the morbidity and mortality are more than one order of magnitude higher than those found for malaria, schistosomiasis or leishmaniasis [2]. Current estimates indicate 200,000 new cases every year and an annual mortality of ~50,000 [2]. On the other hand, Hepatitis C virus (HCV) is a bloodborne infection that affects nearly 2.2% of the world's population, or 130 million people [3]. Approximately 55–85% of newly infected cases progress to chronicity; of those, 20–30% will develop liver fibrosis, cirrhosis, and liver failure and 2–5% will advance to hepatocellular carcinoma [3].

Common chemotherapeutic agents currently used against leishmaniasis and trypanosomiasis are often inadequate since they require long courses of administration, may have toxic side effects or become less effective due to the emergence of resistant strains [1]. On the other hand, the current standard treatment of care for hepatitis C (peginterferon and ribavirin) is effective in about half of all patients treated [4]. Therefore, new, effective and inexpensive drugs that can be used to treat these diseases are urgently required.

The thiazolides represent a novel class of anti-infective drugs, with nitazoxanide [2-acetyloxy-*N*-(5-nitro-2-thiazolyl)benzamide, Alinia®, NTZ] as the parent compound. NTZ is marketed in the US and LA for treating diarrhea and enteritis caused by *Cryptosporidium spp.* or *Giardia lamblia* in adults and children down to 12 months of age [5]. Following oral administration of a 500 mg tablet, NTZ is partially absorbed from the gastrointestinal tract and rapidly hydrolyzed in plasma to form its active circulating metabolite, tizoxanide (TIZ, Fig. 1.), which is as effective as the parent drug [6]. In fact, both NTZ and TIZ are active against *Trypanosoma cruzi* (the causative agent of Chagas disease) and *Leishmania mexicana* [1], and the ulcer-causing pathogen *Helicobacter pylori* [7]. Also, both NTZ and TIZ are potent inhibitors of hepatitis B virus (HBV), and in combination with other antiviral agents such as lamivudine or adefovir show synergistic effects [5]. Additionally, NTZ and TIZ are potent inhibitors of HCV in genotype 1a- and 1b-derived replicon cells and genotype 2a-cell culture models, and synergistic effects are observed when TIZ is combined with interferon [8]. Thus, TIZ is a promising anti-infective agent that may enhance current or future therapies for leishmaniasis, Chagas disease and viral hepatitis caused by HBV or HCV.

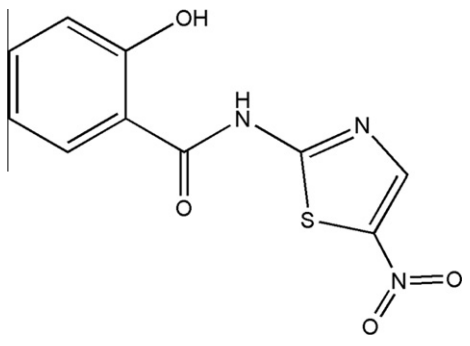

Fig. 1. Chemical structure of tizoxanide (TIZ).

The importance of characterizing the solid-state properties and the absolute configuration of a drug, which is a critical property in biological systems as changes in this may alter the response of the biologic system, has been well documented in the literature. To our knowledge, the experimental data available in the pharmaceutical literature on the solid-state properties of TIZ are the melting point (with two different values reported, *viz.* 254 °C [9] and 279–281 °C [10] and the FTIR spectrum (KBr), which was not thoroughly analyzed and assigned [9,11].

In this report, we describe for the first time, the crystal structure of TIZ as determined by single crystal X-ray diffraction (SXRD). The structural features of TIZ are also discussed in the context of its vibrational [diffuse reflectance infrared Fourier transform (DRIFT) and FT-Raman], spectroscopic [Solid-state (SSNMR) and solution (S NMR) nuclear magnetic resonance spectroscopy] and thermal [differential scanning calorimetry (DSC), thermogravimetry (TG) and hot stage microscopy (HSM)] properties of this compound.

2. Experimental

2.1. Materials

Tizoxanide, designated hereafter as TIZ-rp, was obtained by acid hydrolysis (aqueous HCl 37% w/w, 50 °C, 24 h [8]) of NTZ commercial raw powder (99.89% purity) and was used as such to record the DRIFT, FT-Raman and NMR spectra, as well as the DSC and TG curves. Single crystals were grown from a filtered hot saturated solution of TIZ-rp in dimethylformamide. By slow recrystallization at room temperature (25–30 °C), suitable crystals for X-ray analysis were obtained. All other chemicals and solvents were of analytical reagent grade or spectroscopic quality.

2.2. Single-crystal X-ray structure determination

Table 1 lists crystal data and refinement parameters for TIZ. During data-collection (program COLLECT [12]) the crystal was cooled in a constant stream of nitrogen vapor (Oxford Cryostream, UK). Program DENZO-SMN [13] was used for data-reduction and unit cell refinement. Laue symmetry (-1) indicated the triclinic crystal system and the value of $\langle E-1\rangle = 0.984$ indicated the centric space group $P(-1)$. The structure was solved by direct methods and refined by full-matrix least-squares on F^2 using programs in the SHELX-suite [14]. Following isotropic and anisotropic refinement of the non-hydrogen atoms, all H atoms were located in difference electron density maps and were subsequently included in a riding model with isotropic thermal displacement parameters U_{iso} equal to 1.2 U_{eq} of their parent atoms.

2.3. Differential scanning calorimetry (DSC), thermogravimetry (TG) and hot stage microscopy (HSM)

The DSC and TG measurements were recorded on MDSC 2920 and TG 2950 analyzers (TA Instruments Inc., USA) respectively, at a heating rate of 10 °C/min under N_2 (99.99% purity, flow rate 50 mL/min). For DSC measurements, closed and hermetically-closed aluminum pans were used. The DSC and TG temperature axes were calibrated with indium (99.99% purity, *m.p.* 156.6 °C) and the Curie point of Ni (358.1 °C), respectively. Empty aluminum pans were used as references. Samples with mass 1–2 mg were employed. Data were treated with Universal Analysis 2000 software (TA Instruments Inc.).

The physical and morphological changes that occurred during the process of heating TIZ particles were observed through a microscope fitted with a Kofler hot-stage (Leitz, Wetzlar, Germany) at a constant rate of about 8 °C/min from about 25 °C.

Table 1
Crystal data and refinement parameters for tizoxanide (TIZ).

Chemical formula	$C_{10}H_7N_3O_4S$
Formula weight	265.25
Temperature (K)	173(2)
Wavelength (Å)	0.71073, Mo K
Crystal system	Triclinic
Space group	$P(-1)$ (No. 2)
Unit cell parameters a, b, c (Å), α, β, γ (°)	5.4110(3), 7.3315(6), 13.5293(9), 97.528(3), 95.390(4), 97.316(5)
Volume (Å^3)	524.41(6)
Z	2
Calculated density (Mg m^{-3})	1.680
μ (mm^{-1})	0.320
F_{000}	272
Crystal size (mm^3)	0.13 × 0.16 × 0.20
Diffractometer/ measurement method	Nonius Kappa CCD/ω- and ϕ-scans 1.0°
Index ranges	$-7 \leqslant h (7, -9 \leqslant k \leqslant 9, -17 \leqslant l \leqslant 17$
θ-range for data-collection (°)	$1.00 \leqslant \theta \leqslant 27.48$
Measured reflections	4601
Independent/observed reflections	2374/1910
R_{int}	0.0204
Refinement method	Full-matrix least-squares on F^2
Data/restraints/parameters	2374/0/164
Goodness-of-fit on F^2	1.055
R indices [$I > 2\sigma(I)$]	$R_1 = 0.0339$, $wR_2 = 0.0846$
R indices (all data)	$R_1 = 0.0482$, $wR_2 = 0.0911$
Weighting scheme	$w = 1/[\sigma^2(F_o^2) + (0.0502P)^2 + 0.1025P]$, $P = (F_o^2 + 2F_c^2)/3$
$\Delta\rho_{min}$, $\Delta\rho_{max}$ (e Å^{-3})	−0.27, 0.33

2.4. NMR spectroscopy

^{13}C SSNMR studies were performed using the ramp CPMAS sequence with proton decoupling during acquisition, at 25 °C in a Bruker Avance II 300 spectrometer (Bruker, Germany), operating frequency for carbons 75 MHz, equipped with a 4 mm MAS probe. Spinning rate was 8 kHz. The recycling time was 20 s, the contact time during CP was 2 ms, and 2048 scans were recorded. TPPM15 sequence was used for decoupling during acquisition with a proton field H_{1H} satisfying $\omega_{1H}/2\pi = \gamma_H H_{1H}/2\pi = 50.0$ kHz. Chemical shifts were quoted with respect to tetramethylsilane (TMS) and measured via replacement with adamantane (29.50 and 38.56 ppm). Interrupted decoupled experiments were conducted using a 40 μs delay before acquisition. The complete signal assignments of the spectrum were achieved by dipolar dephasing experiments [which yields quaternary carbons only and the corresponding non-quaternary suppression (NQS) spectrum] and by comparison with one-dimensional solution ^{1}H [spectral width of 20 ppm using a 30° pulse (7.09 μs) and 16 scans] and ^{13}C (100 MHz using the following acquisition parameters: spectral width, 220 ppm; relaxation delay, 1.7 s; 2048 scans for sample, and a 30° excitation pulse). NMR spectra (in DMSO-d_6) of TIZ and NTZ [15] along with two-dimensional COSY-45, HSQC and HMBC spectra [Bruker Avance II 400 spectrometer current probe 5 mm BBI 1H/D-BB Z-GRD Z8202/0349]. The COSY-45 spectrum (DMSO-d_6) was obtained using gradient pulses for selection, and the following acquisition parameters: scans, 2; relaxation delay, 1 s; f1 channel 30° high power pulse (7.09 μs) and sizes of fid of 256 (time domain 1) and 2048 (time domain 2). The HSQC spectrum (DMSO-d_6) was obtained using 4 scans, a relaxation delay of 1 s, a f1 channel 30° high power pulse of 7.09 μs, sizes of fid equal to those of the COSY-45 spectrum, and a one-bond C—H coupling constant of 145 Hz. The HMBC spectrum (DMSO-d_6) was obtained using acquisition parameters identical to those of the H*SQC spectrum but with 8 scans, and more than one-bond C—H coupling constant of 8 Hz was used. The center of the solvent peak was used as an internal standard which was related to TMS. The processing of the data was performed with a Bruker Standard program (TOPSPIN 2.0).

2.5. Diffuse reflectance infrared Fourier transform (DRIFT) and Raman spectroscopy

DRIFT and Raman spectra were recorded on a Nicolet Avatar 360 FTIR spectrometer (Nicolet Instruments Corp., Madison, WI) and a Horiba Jobin Ivon LabRaman HR instrument (Horiba, Kyoto, Japan), respectively. For the DRIFT spectrum, a diffuse reflectance accessory and macro-diffuse reflectance cups of 13-mm diameter (~400 mg capacity) were used. For the preparation of the sample-KBr blend, dry KBr was ground for 2 min before mixing with the sample (2.5% w/w) in an agate mortar with only light grinding performed. The blend was then placed in the cup, and excess material was removed by placement of a microscope slide against the open cup in a rotary motion to leave a level but roughened surface, that was scanned immediately. KBr scans were used as background. The Raman spectrum was acquired operating the instrument at a resolution of 4 cm^{-1}, using a 632.8 nm excitation from a He–Ne laser (at 10% of its power) in the range of 4000–400 cm^{-1}. The data were acquired using back scattering with 1800 grating, 5 scans per 30 s (10 s) pulse and with 10× zoom. The instrument was calibrated with a Si single crystal.

2.6. X-ray powder diffraction (XRPD)

A Philips X'Pert PRO PANalytical powder diffractometer (Philips, The Netherlands) was used. The measuring conditions were: 20–25 °C, Cu Kα1 radiation (λ = 1.54056 Å), 40 kV, 40 mA, step size of 0.02° (2θ), time per step 5 s, time constant 0.03 s, angular range 3–35° 2θ. A 25 mm diameter Si single crystal holder was used and the sample (gently ground) was pressed by means of a clean glass slide to ensure coplanarity of the powder surface with the surface of the holder. Data were treated with the X'PERT Data Viewer diffraction software.

2.7. Solubility estimation

The solubility of TIZ-rp at 25 °C was estimated according to a previously reported procedure [16]. Briefly, an accurately weighed portion of TIZ-rp (2–3 mg) was added to a 10 mL glass vial. Solvent of known volume was added to the vial. The vial was shaken by hand for 5 min. If solid remains, the procedure was repeated until the solid was completely dissolved. Solubility was then bracketed using the total volumes after the last two additions, and it was expressed as the weight of solid divided by volume of the solvent. Solvents used in this study were acetone, acetonitrile, ammonium hydroxide 1 M, benzene, chloroform, dimethylformamide, DMSO, dioxane, ethanol, ethyl acetate, ethyl ether, *n*-hexane, hydrochloric acid 1 M, *iso*-propyl alcohol, methanol, methylene chloride, *n*-pentane, tetrahydrofuran, *t*-butanol, toluene and water.

3. Results and discussion

3.1. Molecular and crystal structure

Selected molecular parameters for TIZ appear in Table 2. Hydrogen bonds are listed in Table 3. Fig. 2 (left) shows the molecular structure of TIZ with the intramolecular N—H···O hydrogen bond indicated by dotted lines. This interaction results in the 5- and 6-membered rings being almost coplanar (angle of intersection of their least-squares [LS] planes = 2.83(7)°). The maximum deviations above and below the LS plane that includes all 18 non-H

atoms are those for atoms O18 [+0.067(1) Å] and O7 [−0.117(1) Å]. Common bond lengths and angles (Table 2) are in excellent agreement with those reported previously for NTZ [15]. The latter molecule is likewise constrained to be nearly planar by the common intramolecular N—H···O hydrogen bond, but the overall level of planarity is somewhat lower than in the TIZ molecule. This can be attributed to the significantly weaker intramolecular N—H···O(acetyloxy) bond in NTZ (N···O = 2.700(2), 2.681(2) Å for two crystallographically independent molecules) than the N—H···O(hydroxyl) bond occurring in TIZ (N···O = 2.646(2) Å).

Table 2
Selected bond distances, bond angles, and torsion angles for TIZ.

Bond lengths (Å)	
S12—C11	1.725(2)
S12—C13	1.723(2)
C13—C14	1.353(2)
C14—N15	1.364(2)
N15—C11	1.325(2)
O7—C1	1.363(2)
O9—C8	1.222(2)
O17—N16	1.234(2)
O18—N16	1.229(2)
Bond angles (°)	
C11—S12—C13	86.39(7)
S12—C13—C14	113.2(1)
C13—C14—N15	113.8(1)
C14—N15 -C11	109.8(1)
N15—C11—S12	116.7(1)
C11—N10—C8	122.1(1)
N10—C8—C2	118.3(1)
O17—N16—O18	123.8(1)
Torsion angles (°)	
C1—C2—C8—N10	5.5(2)
C2—C8—N10—C11	179.4(1)
C8—N10—C11—S12	−2.3(2)
S12—C13—N16—O17	1.3(2)

Table 3
Hydrogen bond parameters for TIZ.[a]

No.	Bond	D···A (Å)	D—H (Å)	H···A (Å)
1	N10—H10···O7	2.646(2)	0.88	1.95
2	O7—H7···N15^{i}	2.757(2)	0.84	1.93
3	C14—H14···O18^{ii}	3.371(2)	0.95	2.43
4	C5—H5···O17^{iii}	3.438(2)	0.95	2.53
5	C3—H3···O9^{iv}	3.448(2)	0.95	2.52

[a] Symmetry operations: (i) −*x*, 1 − *y*, 1 − *z*; (ii) −*x*, 1 − *y*, −*z*; (iii) *x*, *y*, 1 + *z*; (iv) 2 − *x*, 2 − *y*, 1 − *z*.

The planarity of the TIZ molecule is further manifested in its remarkable ability to form infinite layers *via* extensive intermolecular O—H···N and C—H···O hydrogen bonding. In the representative portion of such a layer shown in Fig. 2 (right), the unique hydrogen bonds are labelled **1**–**5** (as in Table 3) while individual ring motifs are labelled ***a***–***e***. H-bond **1** is the intramolecular interaction that results in the ring motif ***a***, with graph-set notation $S(6)$ [17]. The remaining rings with their graph-set descriptors and the H-bond combinations that generate them are as follows: ring ***b*** [$R_4^4(12)$, containing two O—H···N and two N—H···O hydrogen bonds], ring ***c*** [$R_2^2(10)$, containing two C—H···O(nitro) H-bonds], ring ***d*** [$R_3^3(12)$, containing one O—H···N and two C—H···O(nitro) H-bonds], and the large ring ***e*** [$R_4^4(26)$, formed by the combination of two C—H···O(carbonyl) and two C—H···O(nitro) H-bonds]. The layer is thus constructed from the co-operative effects of a series of stable, hydrogen-bonded ring motifs of different topologies and the TIZ molecules are closely packed within the layer. The hydrogen bonding capacity of the TIZ molecule is fully utilized in such layer formation and a stable crystal is formed by close stacking of such layers *via* strong π–π interactions between the phenyl group of a TIZ molecule and the thiazolyl ring of a centrosymmetrically-related molecule. There are two unique interactions of this type, with distances between the ring-centroids of 3.601(1) and 3.807(1) Å. The resulting 'graphitic' structure is illustrated in Fig. 3, which shows three layers in both stick and space-filling mode.

The refined single crystal X-ray data were used to compute the idealized X-ray powder pattern [18] for this crystalline phase at 173 K (Fig. 4a). As expected, the peak of highest intensity (at $2\theta = 27.9°$) corresponds to reflection of X-rays from the layers highlighted in Fig. 3, these layers coinciding with the crystal planes (1 2 0) whose interplanar spacing (d) is 3.2 Å at 173 K. We note that the interlayer distance is therefore remarkably short and it is significantly smaller than the distances cited above between the relevant ring centroids as a result of large offsets between the π-stacked phenyl and thiazolyl rings. The relative 'simplicity' of the crystal structure of TIZ leads to only four very prominent peaks at 2θ-values 6.6°, 16.6°, 24.7° and 27.9°, the remaining peaks having significantly lower intensities. The calculated pattern is in good agreement with the experimental one (Fig. 4b), confirming that there is no significant structural change when the crystal was cooled from ambient laboratory temperature (294 K) to 173 K.

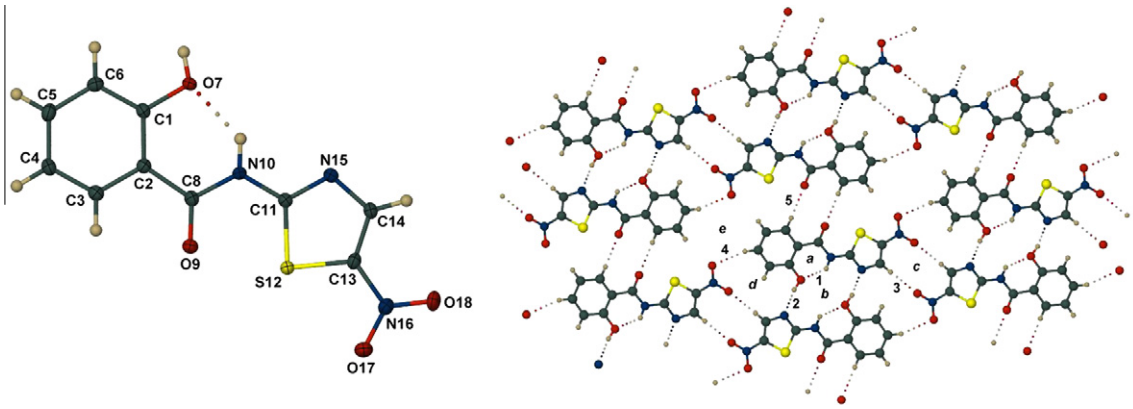

Fig. 2. Molecular structure and conformation of TIZ with non-H atoms shown as thermal ellipsoids drawn at the 50% probability level and H atoms shown as spheres of arbitrary radii (left) and extensive hydrogen bonding within a layer of TIZ molecules (right).

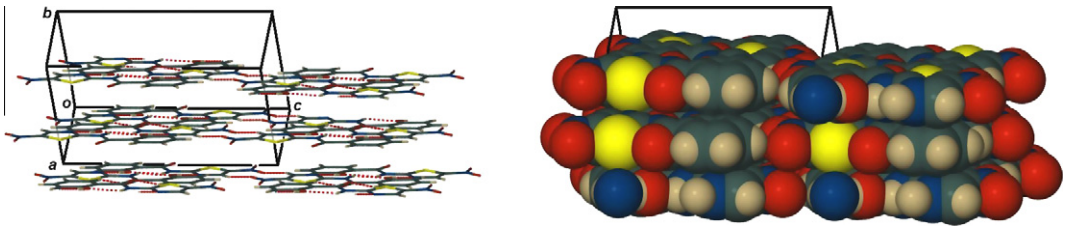

Fig. 3. Portions of three stacked layers of TIZ represented in stick mode (left) and space-filling mode (right). The interlayer distance is ~3.2 Å.

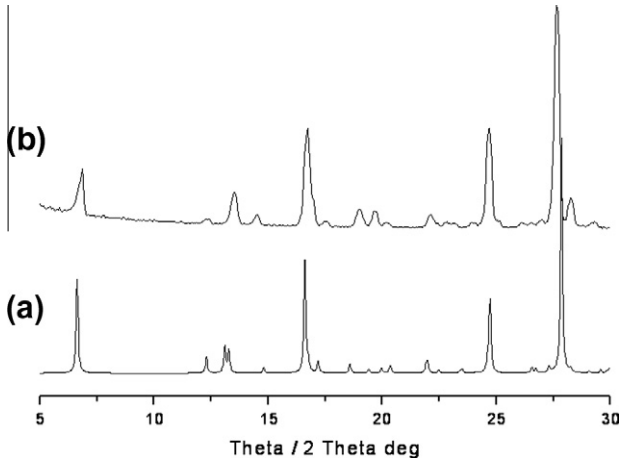

Fig. 4. (a) Computed XRPD trace of TIZ calculated at 173 K and (b) experimental diffractogram of TIZ-rp.

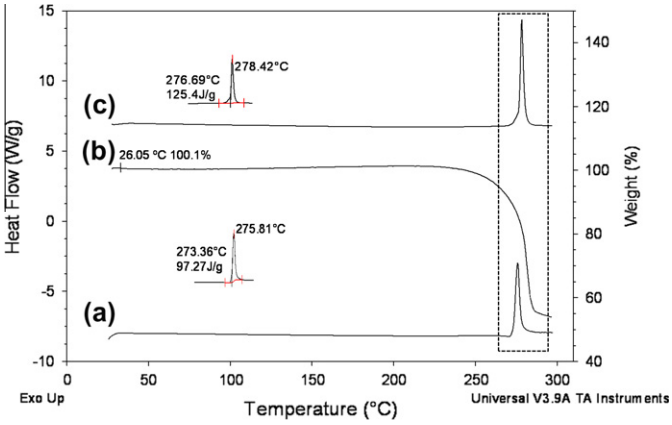

Fig. 5. Overlaid DSC and TG traces of TIZ-rp (10 °C/min, flowing N_2 at 50 mL/min): (a) DSC curve in crimped pan, (b) TG curve (open pan) and (c) DSC trace in hermetically sealed pan. Insets: DSC peaks.

Subsequent to the above analysis, we were alerted to a recent report of the X-ray crystal structure of the TIZ pyridine monosolvate [19] and we carried out a detailed comparison of the structures of the drug molecule in the crystal of pure TIZ and the solvated species. In both crystals the TIZ molecule is essentially planar, the co-planarity of the two rings being maintained by the common intramolecular N—H···O bond. The latter is slightly stronger in the solvated phase (N···O 2.625(2) Å compared with 2.646(2) Å in the crystal of pure TIZ). Covalent bond distances in the TIZ molecule do not, however, differ significantly in the two phases. Finally, in the TIZ pyridine monosolvate structure, the drug and included solvent molecules are linked by a O—H···N bond, with the molecular planes of the TIZ molecule and the pyridine molecule almost orthogonal, thus precluding the unusual 'graphitic'-type structure reported here for pure TIZ.

3.2. Thermal, vibrational and spectroscopic data

The overlaid DSC and TG curves of TIZ-rp are shown in Fig. 5. The DSC and TG curves obtained in closed and open pans respectively (Fig. 5a and b) showed neither endothermic peaks nor TG mass losses in the 25–240 °C temperature range, confirming the absence of solvates or residual solvent, in accord with the SXRD data that revealed that TIZ was unsolvated. Above 260 °C, the DSC curve (Fig. 5a) exhibited a barely discernible endothermic event superimposed on a sharp exothermic peak at 273.4 °C (Extrapolated onset temperature, Tonset), ascribable to an exothermic decomposition process. The corresponding TG curve (Fig. 5b) showed a mass loss of about 45% that coincided with the DSC endo-exothermic events and it occurred in one-step between 230 and 300 °C, confirming the decomposition of TIZ. In addition, a DSC baseline shift was noted after the exothermic peak, and this was consistent with changes in the sample mass [20], as indicated by TG. On the other hand, the DSC trace of TIZ-rp obtained in a hermetically-closed pan (Fig. 5c) showed only a sharp exothermic peak at 276.7 °C (Tonset), which exhibited no baseline shift probably because the sample mass did not change, as volatile decomposition products were not formed or they could not escape due to the hermetic encapsulation. The absence of an endothermic peak and the small upward shift of the exothermic one (from 273.4 to 276.7 °C) as the pan system changed from closed (Fig. 5a) to hermetically-closed (Fig. 5b) evidently indicates that the thermal decomposition of TIZ is affected by the sample encapsulation.

Taking into account that no sharp, isolated melting peak was detected for TIZ-rp in either type of pan, observations under a Kofler apparatus were made to identify whether or not there had been melting, perhaps local and temporary, during decomposition. On heating from 25 to 270 °C, the colorless transparent irregular particles of TIZ-rp (Supplementary material) did not undergo changes in shape, color or size, and no vapor condensation on the cover slip was noted, discarding the occurrence of phase transitions or evaporation losses, and this was consistent with the DSC and TG results. At about 275 °C, the crystalline particles of TIZ-rp started to bubble, lose their shape and darken simultaneously. Consequently, after cooling the slide, a gummy dark-brown residue was obtained, confirming the thermal decomposition of the sample. According to these HSM results, melting of TIZ-rp did not occur before its exothermal decomposition to yield a single coherent droplet and an isolated DSC melting peak. Local and temporary melting probably occurred, as indicated by the detection of bubbles and sintering, which is evidence that surface free-energy (liquid) forces control textural features resulting in surface area minimization [21].

The ^{13}C CPMAS and the NQS spectra of TIZ-rp are shown in Fig. 6, while the carbon assignments and chemical shift values are given in Table 4. The CPMAS spectrum (Fig. 6a) exhibited nine signals for the ten carbons of the molecule, indicating that one of

them corresponded to two carbons, *i.e.* the signal at 163.1 which was assigned to the C-8 carbonyl and the C-11 carbon. The NQS spectrum (Fig. 6b) showed four signals, indicating that the peaks observed in the CPMAS spectrum in the range 116–140 ppm corresponded to the five C—H carbons of the molecule, *i.e.* the four benzenoid carbons and C-14. The ^{13}C SSNMR spectrum was also compared with that recorded in DMSO-d_6 solution and the data appear in Table 4. It is clear that the chemical shifts of five carbon atoms of the molecule, C-4, C-5, C-6, C-11 and C-13, measured in the solid-state have values close to those observed in solution (the differences in chemical shifts were all less than ±1.5 ppm), indicating that the chemical environment around these carbons is very similar in the solid-state and in solution. In contrast, the C-1, C-2, C-3, C-8 and C-14 chemical shifts measured in the solid-state are slightly different from those observed in DMSO-d_6. The chemical shifts of atoms C-1, C-2 and C-8 are shifted to a low frequency in the solid state (Δsolid-solution: −2.3, −3.5 and −3.0 ppm, respectively), and since these carbons are close to the intramolecular N—H···O bond, the shifts could be attributed to the replacement of intramolecular H-bonding by intermolecular H-bonds with DMSO-d_6 molecules through the amide and/or OH protons [22]. In contrast, the chemical shift of the C-3 carbon was shifted to a high frequency in the solid-state, and this could indicate a small change in the orientation of the amide group in the solid-state with respect to the DMSO solution, as was also observed for NTZ [15]. With regard to C-14, very similar chemical shifts are observed for C-13 and C-14 in the ^{13}C S NMR spectrum (Table 4), indicating a chemical similarity of these carbons; however, two separate signals at 143.5 and 138.1 ppm with an accompanying low frequency shift of −3.8 ppm for the C-14 chemical shift is observed for this carbon in the solid state, indicating that the chemical environments are different for these carbon atoms, possibly due to further rigidities of the nitro group and thiazole ring in the solid state, as was also observed for NTZ [15].

The DRIFT and FT-Raman spectra (Fig. 7) were also compared to obtain additional information regarding the intra- and intermolecular interactions in TIZ-rp. The origins of the major peaks of both spectra were assigned using published compilations and literature studies [23–28]. As characteristic features, the DRIFT spectrum (Fig. 7a) showed a strong NH stretch absorption centered at 3253.8 cm^{-1}, which is superimposed on a broad band ranging from 3500 to 2250 cm^{-1}. Neither band seems to have a counterpart in the Raman spectrum (Fig. 7b). In the absence of H-bonding, it would be reasonable to assume that the amide N—H stretching mode would be observed above 3300–3500 cm^{-1} [23]. The shift to lower wavenumbers observed in the DRIFT spectrum indicates that the NH group is associated through H-bonding, which is in good agreement with the determined crystal structure of TIZ. Indeed, in the crystal, the amide group hydrogen is involved in a strong intramolecular hydrogen bonding interaction of the NH···O type with the oxygen atom of the C1-OH group. The high intensity of the NH vibration is additional evidence of such intramolecular interaction [27], as well as for presence of a planar —CONH group [28]. In fact, the FTIR spectra of various benzamides with ortho-ring substituents that formed intramolecular H-bonds with polar groups, like the phenolic C1-OH group of TIZ [27], and displayed planar —CONH groups, did exhibit strong NH vibrations [28].

The absence of a separate —OH stretching vibration in the DRIFT spectrum (Fig. 7a) also confirms the participation of the —OH proton in H-bonding since such interaction leads to a red shift of the —OH stretching band and to a broad continuum in the 3200–2500 cm^{-1} range [29]. According to the SXRD data, a classical O—H···N intermolecular H-bond is formed between the C1-OH group of one molecule of TIZ and the thiazolic nitrogen of a symmetry-related molecule (Fig. 2), which is well evidenced in the DRIFT spectrum by the broad —OH continuum in the range 3500–2300 cm^{-1}. On the other hand, the absence of the —OH stretching band in the Raman spectrum (Fig. 7b) is characteristic and offers a window to the weak CH stretching bands that are buried below the —OH continuum in the FTIR spectrum [29]. Thus, both spectra exhibited bands at 3115.9 and 3071.1 cm^{-1} (DRIFT) and 3114.3 and 3072.2 cm^{-1} (Raman), ascribable to the aromatic C—H stretching vibrations that are normally found between 3100 and 3000 cm^{-1} [23].

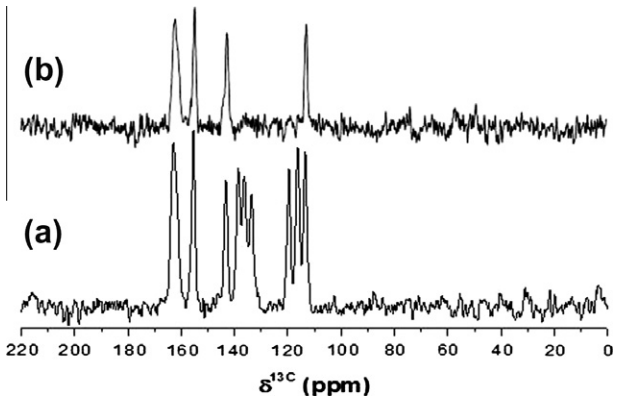

Fig. 6. (a) ^{13}C SS CPMAS and (b) NQS spectra of TIZ-rp.

Table 4
Comparison of the ^{13}C NMR chemical shifts (in ppm) of TIZ-rp in the solid state (CPMAS spectrum) and in solution (DMSO-*d*6).

C atom	CPMAS spectrum	DMSO-d_6 (0.065 M)	Difference (SS-DMSO-d_6)
1	155.5	157.8	−2.3
2	113.6	117.1	−3.5
3	133.3	130.9	2.4
4	119.6	120.3	−0.7
5	136.3	135.5	0.8
6	116.4	117.6	−1.2
8	163.1	166.1	−3.0
11	163.1	162.1	1.0
13	143.3	142.8	0.5
14	138.6	142.4	−3.8

In the solid state (CPMAS spectrum) and in solution (DMSO-d_6).

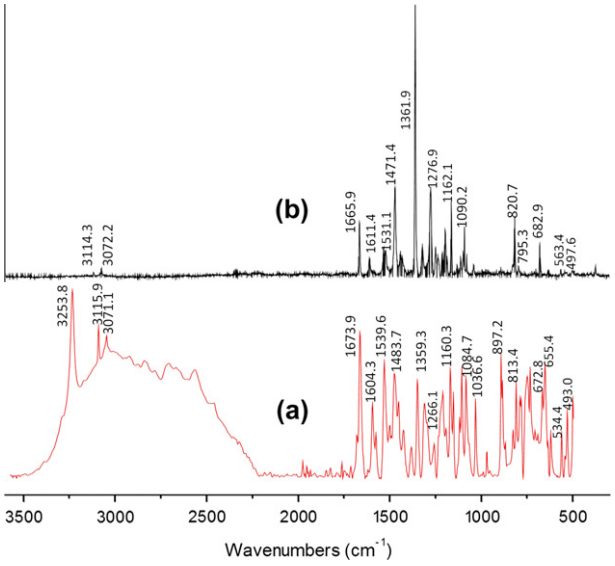

Fig. 7. (a) DRIFT (KBr) and (b) Raman (632.8 nm excitation, He–Ne laser) spectra of TIZ-rp.

Table 5
Estimated solubility of TIZ in various solvents at 25 °C.

Solvent	Solubility (mg/mL)
Acetone	0.38
Acetonitrile	Insoluble
Ammonium hydroxide 1 M	Insoluble
Benzene	Insoluble
Chloroform	Insoluble
Dimethylformamide	3.00
DMSO	4.50
Dioxane	2.00
Ethanol	Insoluble
Ethyl acetate	Insoluble
Ethyl ether	Insoluble
Hydrochloric acid 1 M	Insoluble
Iso-Propyl alcohol	Insoluble
Methanol	Insoluble
Methylene chloride	Insoluble
n-Hexane	Insoluble
n-Pentane	Insoluble
t-Butanol	Insoluble
Tetrahydrofuran	Insoluble
Toluene	Insoluble
Water	Insoluble

Also present in the spectra were bands at 1673.9 (DRIFT) and 1665.9 cm^{-1} (Raman) assigned to the amide carbonyl (8-C=O) stretch, and 1539.6 cm^{-1} in IR and at 1531.1 cm^{-1} in the Raman spectra, respectively, ascribed to the C—(NO_2) asymmetric stretching of TIZ. The in-plane bending mode of the —OH group, normally observed in the region 1250–1150 cm^{-1}, is observed at 1160.3 (DRIFT) and 1162.1 (Raman) cm^{-1}. The vibrations at 1359.3 (DRIFT) and 1361.9 cm^{-1} (Raman) were assigned tentatively to the amide C—N stretch overlapped with the symmetrical mode of the NO_2 group, and to the amide N—H bend and the asymmetrical stretch of the NO_2 group, respectively. Also visualized in the DRIFT spectrum are medium bands at 897.2 and 813.4 cm^{-1}, which were assigned to the aromatic C—H out-of-plane bending vibrations of TIZ; whereas the bands at 672.8 and 655.4 (DRIFT) and 682.9 (Raman) cm^{-1} were assigned to the CCC in-plane bending mode [28].

3.3. Solubility estimation

The estimated solubility of TIZ rp in 21 solvents at 25 °C is shown in Table 5. The obtained data showed that TIZ-rp is very slightly soluble in acetone (0.38 mg/mL); slightly soluble in dimethylformamide, DMSO and dioxane (3, 4.5 and 2 mg/mL respectively), and practically insoluble in water and the rest of the tested solvents, according to the USP solubility terms [30]. The insolubility of TIZ-rp in water is consistent with the crystal and molecular structure of TIZ determined by SXRD since It is well known that when a compound can assemble into a highly ordered crystal it tends to have low solubility in aqueous media [31]. This modification of TIZ has a 'graphitic' structure composed of tightly packed layers of hydrogen bonded molecules that are stacked on top of one another and held together by strong π-stacking interactions, factors which evidently determine that TIZ-rp cannot be solubilized by aqueous media and polar protic solvents, at least at 25 °C.

4. Conclusions

By combining the results of the single crystal XRD analysis of TIZ with those from ^{13}C SS CPMAS, DRIFT and FT Raman spectra, DSC, TG as well as estimated solubility data at 25 °C, it was possible to characterize comprehensively for the first time the solid-state characteristics of TIZ. X-ray structural investigation of TIZ shows that the analyzed modification has a 'graphitic' structure composed of tightly packed layers of hydrogen bonded molecules that are stacked on top of one another and held together by strong π-stacking interactions between the phenyl and thiazolyl rings of inversion-related TIZ molecules. This is an exceptionally good example of layer formation that involves the interlocking of a series of stable ring structures created by extensive hydrogen bonding. DRIFT and FT-Raman studies indicate that the vibrational spectra of TIZ-rp exhibit features characteristic of a hydrogen bonded molecule, confirming the intra- and intermolecular interactions as revealed by the resolved crystal structure. Thermal analysis has been used to further characterize TIZ-rp, and the information obtained from the DSC and TG curves was that solid TIZ has relatively high thermal stability, *i.e.* the Tonset is higher than 270 °C, and that melting is not an isolated event from the one-step exothermic decomposition that this modification undergoes.

Acknowledgements

Financial support from SECyT-UNC and FONCyT of Argentina is gratefully acknowledged. F.P. Bruno acknowledges financial support from FONCyT and CONICET fellowships. Helpful comments on NMR solution spectra from Dra. G. Bonetto, who recorded the spectra, are gratefully acknowledged. MRC thanks the University of Cape Town and the National Research Foundation (Pretoria) for research support. Thanks also go to Prof. Dr. E. Coronado (Departamento de Fisicoquímica, FCQ, UNC) for the use of Micro-Raman facilities.

Appendix A. Supplementary material

CCDC 857093 contains the supplementary crystallographic data for this paper. These data can be obtained free of charge at www.ccdc.cam.ac.uk/ retrieving.html [or from the Cambridge Crystallographic Data Centre (CCDC), 12 Union Road, Cambridge CB2 1EZ, UK; fax: +44(0)1223-336033; email: deposit@ccdc.cam.ac.uk]. Supplementary data associated with this article can be found, in the online version, at http://dx.doi.org/10.1016/j.molstruc.2012.12.004.

References

[1] M.J. Chan-Bacab, E. Hernández-Núñez, G. Navarrete-Vázquez, J. Antimicrob. Chemother. 63 (2009) 1292.
[2] E.L. Romero, M.J. Morilla, Adv. Drug Deliv. Rev. 62 (2010) 576.
[3] S.S. El-Kamary, R. Jhaveri, M.D. Shardell, Clin. Infect Dis. 53 (2011) 150.
[4] R.P. Ward, M. Kugelmas, Am. Fam. Physician 72 (2005) 655.
[5] B.E. Korba, A.B. Montero, K. Farrar, K. Gaye, S. Mukerjee, M.S. Ayers, J.-F. Rossignol, Antiviral Res. 77 (2008) 56.
[6] J.-F. Rossignol, J.E. Semple. Romark Laboratories, LC, United States Patent No. 8,124,632 B2, 2012.
[7] F. Mégraud, A. Occhialini, Antimicrob. Agents Chemother. 42 (1998) 2836.
[8] B.E. Korba, M. Elazar, P. Lui, J.-F. Rossignol, J.S. Glenn, Antimicrob. Agents Chemother. 52 (2008) 4069.
[9] J.-F. Rossignol, F. Clearwater. Romark Laboratories, LC United States Patent No. 6,020,353,2000 <http://www.ptodirect.com/Results/Patents?query=PN/6020353>.
[10] Zhejiang NetSun Co., ChemNet.CAS: 173903-47-4 Tizoxanide. <http://www.chemnet.com/cas/supplier.cgi?terms=tizoxanide&l=&exact=dict&f=plist&mark=&submit.x=0&submit.y=0&submit=search>.
[11] M. Donadel Malesuik, H. Mazzotti Lopes Goncalves, C.V. Garcia, M. Rodrigues Trein, N. Beyer Nardi, E.E. Scherman Schapoval, M. Steppe, Talanta 93 (2012) 206.
[12] COLLECT, Nonius, Nonius BV, Delft, The Netherlands, 1998.
[13] Z. Otwinowski, W. Minor, in: M.G. Rossman, E. Arnold (Eds.), International Tables for Crystallography, vol. F, Kluwer, Dordrecht, 2000.
[14] G.M. Sheldrick, Acta Crystallogr. A 64 (2008) 112.
[15] F.P. Bruno, M.R. Caira, G.A. Monti, D.E. Kassuha, N.R. Sperandeo, J. Mol. Struct. 984 (2010) 51.
[16] C.C. Sun, Int. J. Pharm. 319 (2006) 114.
[17] M.C. Etter, J.C. MacDonald, J. Bernstein, Acta Crystallogr. 46 (1990) 256.
[18] K. Yvon, W. Jeitschko, E. Parthe, J. Appl. Crystallogr. 10 (1977) 73.

[19] H. Zheng, H. Deng, Y. Chen, D. Li, Acta Crystallogr. E68 (2012) o1453.
[20] L.C. Thomas, TA-039: Interpreting Unexpected Events and Transitions in DSC Results. TA Instruments, New Castle, DE. <http://www.tainst.com> (accessed 15.05.12).
[21] A.K. Galwey, J. Therm. Anal. 41 (1994) 267.
[22] M. Kondo, Bull. Chem. Soc. Jpn. 52 (1979) 521.
[23] R.M. Silverstein, F.X. Webster, D.J. Kiemle, Spectrometric Identification of Organic Compounds, seventh ed., John Wiley & Sons, Inc., NJ, 2005.
[24] C. Gobin, P. Marteau, J. Petitet, Spectrochim. Acta A 60 (2004) 329.
[25] Y. Akkaya, S. Akyuz, Vib. Spectrosc. 42 (2006) 292.
[26] H.T. Varghese, C. Yohannan Panicker, D. Philip, J.R. Mannekutla, S.R. Inamdar, Spectrochim. Acta A 66 (2007) 959.
[27] V. Arjunan, M. Kalaivani, P. Ravindran, S. Mohan, Spectrochim. Acta A 79 (2011) 1886.
[28] J.L. Castro, M.R. Lopez-Ramirez, J.F. Arenas, J. Soto, J.C. Otero, Langmuir 28 (2012) 8926.
[29] P.E. Hansen, J. Spanget-Larsen, in: Zvi Rappoport (Ed.), NMR and IR Spectroscopy of Phenols in the Chemistry of Phenols, John Wiley & Sons, NJ, 2004.
[30] The United States Pharmacopeia, 32th ed., United States Pharmacopeial Convention, Inc., 2008.
[31] V. Hayden Thomas, S. Bhattachar, L. Hitchingham, P. Zocharski, M. Naath, N. Surendran, C.L. Stoner, A. El-Kattan, Exp. Opin. Drug Metab. Toxicol. 2 (2006) 591.